Ab initio study of the volume dependence of dynamical and thermodynamical properties of silicon

G.-M. Rignanese, J.-P. Michenaud, and X. Gonze
Unité de Physico-Chimie et de Physique des Matériaux, Université Catholique de Louvain, 1 Place Croix du Sud, B-1348 Louvain-la-Neuve, Belgium
(Received 2 August 1995; revised manuscript received 6 September 1995)

Motivated by the negative thermal expansion observed for silicon between 20 K and 120 K, we present an *ab initio* study of the volume dependence of interatomic force constants, phonon frequencies of transverse-acoustic TA(X) and TA(L) modes, and of the associated mode Grüneisen parameters. The influence of successive nearest-neighbor shells is analyzed. Analytical formulas, taking into account interactions up to second-nearest neighbors, are developed for phonon frequencies of TA(X) and TA(L) modes and the corresponding mode Grüneisen parameters. We also analyze the volume and pressure dependence of various thermodynamic properties (specific heat, bulk modulus, and thermal expansion), and point out the effect of the negative mode Grüneisen parameters of the acoustic branches on these properties. Finally, we present the evolution of the mean-square atomic displacement and of the atomic temperature factor with the temperature for different volumes, for which the anomalous effects are even greater.

INTRODUCTION

In the past few years, theoretical and algorithmic advances have made it possible to determine the thermodynamical properties of solids (such as the specific heat or thermal-expansion coefficient) from first principles calculations.[1,2]

Silicon is a choice system for testing these methods, since accurate measurements on high-purity samples exist over a wide range of temperatures. Moreover, it presents a negative thermal-expansion coefficient between 20 K and 120 K which is of fundamental interest. This unusual thermal-expansion behavior can be attributed to the negative Grüneisen parameters (i.e., phonon frequency increases as crystal volume increases) of the transverse-acoustic (TA) phonons near the Brillouin-zone boundary. It is interesting to note that this anomalous behavior also affects other properties of silicon, such as the mean-square atomic displacement (as shown later in this paper).

This anomalous negative thermal expansion has been analyzed in previous studies, most of them relying on the quasiharmonic approximation.[3] In this approach, the volume dependence of phonon frequencies must be determined. Kagaya, Shuoji, and Soma[4] used a perturbation treatment with a model pseudopotential to calculate the specific heat and the thermal-expansion coefficient. Biernacki and Scheffler[5] employed a Keating model with two parameters, which were extracted from local-density pseudopotential calculations, to compute the thermal-expansion coefficient. Fleszar and Gonze[6] performed a model-free computation of the thermal expansion, using a linear-response technique within density-functional theory.[7] Xu *et al.*[8] used a tight-binding model to calculate the thermal-expansion coefficient and mode Grüneisen parameters; they also showed by using a simple model that the negative values of the mode Grüneisen parameter could be attributed to a larger contribution from the central part of forces than the angular part of forces. More recently, Wei, Li, and Chou[9] extracted interatomic force constants from *ab initio* calculations of planar forces,[10] and calculated the specific heat, the overall Grüneisen parameter, and the thermal-expansion coefficient.

In this paper, we use a variational approach to density-functional perturbation theory to calculate the volume-dependent dynamical properties of silicon (see Sec. I). We present an *ab initio* study of the volume dependence of interatomic force constants up to 25th nearest neighbors. Wei and Chou had also presented such a calculation but only for one volume and up to eighth-nearest neighbors.[10,11] Phonon frequencies of TA(X) and TA(L) modes, and of the associated mode Grüneisen parameters are also calculated for different volumes. The influence of successive nearest-neighbor shells is analyzed. We confirm that the contribution of atoms connected by the zigzag chain along the [1 1 0] direction is the most important, as suggested by Mazur and Pollmann.[12] But we show that the contributions of the fifth, sixth, and seventh atoms along the chain (respectively 13th, 18th, and 25th nearest neighbors) are not negligible, contrary to what had been speculated by Wei and Chou.[10] Analytical formulas, taking into account interactions up to second-nearest neighbors, are developed for phonon frequencies of TA(X) and TA (L) modes and the corresponding mode Grüneisen parameters. In Sec. II, we analyze the volume and pressure dependence of various thermodynamic properties (specific heat, bulk modulus, and thermal expansion). The effect of zero-point motion on static equilibrium properties (lattice constant and bulk modulus) is also analyzed. We point out the effect of the negative mode Grüneisen parameters of the acoustic branches on these properties. In Sec. III, we present the evolution of the mean-square atomic displacement and of the atomic temperature factor with the temperature for different volumes. Anomalous effects present at all temperatures are investigated, using a band-by-band decomposition. Finally, we present our conclusions in the last section.

I. DYNAMICAL PROPERTIES

A. Interatomic force constants

To obtain accurate interatomic force constants (IFC's), we first calculate from first principles the dynamical matrices for ten different wave vectors in the irreducible Brillouin zone (IBZ) (the special points mentioned in Ref. 13) using a variational approach to density-functional perturbation theory.[14] Then, we perform a Fourier transform of these dynamical matrices in order to get the IFC's, following Refs. 1 and 15. This sampling of dynamical matrices allows us to obtain IFC's in a real space box containing 512 atoms. This is more accurate than what had been done in Ref. 6, where the IFC's had only been calculated for two different wave vectors in the IBZ, which corresponds to a real space box of 64 atoms. It is also better than the work of Wei and Chou,[10,11] who had included interatomic interactions up to eighth-nearest neighbors, which corresponds to 99 atoms.

Our calculations, performed within the local-density approximation (LDA),[16] use a preconditioned conjugate gradient algorithm.[17,18] We use a rational polynomial parametrization of the exchange-correlation energy functional,[19] which is based on the Ceperley-Alder gas data.[20] The electronic wave functions are sampled on a mesh of ten special k points in the IBZ and expanded in terms of a set of plane waves whose kinetic energy is limited to 10 hartree. The ''all-electron'' potentials are replaced by an *ab initio*, separable, norm-conserving pseudopotential built following the scheme proposed in Ref. 21. The calculated equilibrium lattice constant is 10.18 bohrs (Ref. 22) (the influence of the zero-point motion on this value will be discussed in Sec. II), whereas the experimental one is 10.26 bohrs.

The calculation of IFC's is performed for three different volumes, corresponding to lattice constants a of 10.00, 10.18, and 10.26 bohrs, respectively. The IFC's for these different lattice constants are listed in Table I, in which coordinates are in units of $a/4$ and notations for the force constants follow Ref. 23.

In Table I, the results are presented with a precision of 10^{-5} hartree/bohr^2. However, we did not analyze the influence on the IFC of changing either the pseudopotential or the exchange-correlation potential. Thus, it has to be noted that the conclusions drawn hereafter hold only for the specific pseudopotential and exchange-correlation potential used in our calculations.

As already noticed in Refs. 10 and 12, IFC's for atoms connected by the zigzag chain along the [1 1 0] direction (or the directions related to it by symmetry) are the most important. The magnitude of IFC's along these peculiar directions decays quite slowly. The contribution of the first nearest neighbors (α_1 and β_1) is about four to five times smaller than the on-site contribution (α_0). Going up to second-nearest neighbors reduces the IFC's by another factor of 5 (λ_2) or 10 (μ_2 and ν_2). The contribution λ_{25} of the seventh atoms along the chain [coordinates (7,7,1) in units of $a/4$], which are already the 25th nearest neighbors, is still of the order of 1% of the contribution of the first-nearest neighbors, and of 5% of that of the second ones. Comparatively, the biggest contribution of the seventh-nearest neighbors (these do not belong to the chain, but are twice as close as the seventh atoms along the chain) is about two times smaller.

In order to visualize these IFC's, we compute the forces induced along the zigzag chain by the displacement of a generic atom of this chain in three perpendicular directions (along [1 1 0], parallel to the chain direction, along [0 0 1], perpendicular to the chain direction; but in the plane of the chain, and along [1 $\bar{1}$ 0], perpendicular to the chain direction, but out of the plane of the chain), all the other atoms being kept fixed. These forces can easily be obtained from IFC's by

$$F_{\kappa\alpha} = -\Phi_{\alpha\beta}(\kappa;\kappa')(R-R_0)_{\kappa'\beta}, \tag{1}$$

where $\mathbf{R}-\mathbf{R}_0$ is the displacement of the generic atom, and the IFC $\Phi_{\alpha\beta}(\kappa;\kappa')$ is the force exerted on ion κ in the direction α due to the displacement of ion κ' in the direction β.

The resulting forces have been reproduced in Fig. 1. The directions of the forces induced by the displacement of the generic atom in the [1 1 0] and [0 0 1] directions show that the bonds along the chain will tend to bend in order to keep constant the bond angles: at sufficient distance, the forces are nearly perpendicular to the last connecting bond. The decay of the magnitude of these forces along the chain is similar to that of the IFC's. On the contrary, the forces induced by the displacement in the [1 $\bar{1}$ 0] direction are much smaller. Indeed, they have the generic form $(\mu-\nu,\nu-\mu,0)$, where μ and ν are of the same order of magnitude (see Table I). It is thus more difficult to interpret them.

B. TA(X) and TA(L) phonon frequencies and associated mode Grüneisen parameters

In previous studies, the negative mode Grüneisen parameters associated with the modes of the acoustic branches, near the zone boundaries, has been shown to drive the negative thermal expansion. We now focus on the analysis of the high symmetry TA(X) and TA(L) modes because analytical results can be obtained for them.

The phonon frequencies can be calculated by solving the dynamical equation

$$\sum_{\kappa'\beta} \Phi_{\alpha\beta}(\kappa;\kappa')u_\sigma(\kappa'\beta) = M_\kappa \omega_\sigma^2 u_\sigma(\kappa\alpha), \tag{2}$$

where $u_\sigma(\kappa\alpha)$ is the displacement in the direction α of ion κ for the normal mode σ, M_κ is the mass of ion κ, and ω_σ is the frequency of the normal mode σ.

In order to analyze the influence of the successive nearest-neighbor shells for TA(X) and TA(L) modes, we artificially limit the interactions taken into account in the IFC matrix $\Phi_{\alpha\beta}(\kappa;\kappa')$ of Table I to the atoms whose distance is less than a cutoff radius. Then, we increase the cutoff radius shell by shell until the sphere contains all the atoms included in the real space box defined by our sampling of the Brillouin zone.

In truncating the interaction to different shells, we break the acoustic sum rule (which states that moving all atoms as a whole should not create any force) unless it is reimposed by artificially changing the on-site IFC α_0.[24] We analyzed the results obtained both with and without reimposing the acoustic sum rule and found no significant difference regarding the convergence with respect to the number of nearest-

TABLE I. Interatomic force constant matrix elements and associated force Grüneisen parameters for silicon at three different volumes, corresponding to lattice constants a of 10.00, 10.18, and 10.26 bohrs, respectively. The convention of Ref. 23 for labeling the matrix elements has been followed. One atom is at the origin, while the coordinates of the second atom are expressed in units of $a/4$; the asterisks indicate the atoms belonging to the zigzag chain along the [1 1 0] direction. The first column indicates the number of the shell NN to which the second atom belongs. The force Grüneisen parameters of IFC matrix elements that are smaller than 10^{-4} hartree/bohr^2 are not mentioned. The interatomic force constant matrix elements are expressed in hartree/bohrs^2.

NN	Coordinate		$a=10.00$	$a=10.18$	$a=10.26$		$a=10.00$	$a=10.18$	$a=10.26$
0	(0,0,0)*	α_0	0.15629	0.13904	0.13201	$\gamma(\alpha_0)$	1.0766	1.1034	1.1047
1	(1,1,1)*	α_1	-0.03779	-0.03385	-0.03225	$\gamma(\alpha_1)$	1.0215	1.0336	1.0275
		β_1	-0.02880	-0.02348	-0.02137	$\gamma(\beta_1)$	1.8264	1.9817	2.0338
2	(2,2,0)*	μ_2	-0.00203	-0.00182	-0.00173	$\gamma(\mu_2)$	0.9600	1.0682	1.1216
		ν_2	-0.00200	-0.00178	-0.00168	$\gamma(\nu_2)$	1.0879	1.1641	1.1951
		δ_2	0.00120	0.00111	0.00108	$\gamma(\delta_2)$	0.6487	0.6997	0.7234
		λ_2	0.00445	0.00433	0.00428	$\gamma(\lambda_2)$	0.2476	0.2456	0.2437
3	$\overline{(1,1,3)}$	μ_3	0.00035	0.00032	0.00031	$\gamma(\mu_3)$	0.6911	0.8662	0.9617
		ν_3	-0.00033	-0.00035	-0.00036	$\gamma(\nu_3)$	-0.6046	-0.5696	-0.5546
		δ_3	0.00032	0.00029	0.00028	$\gamma(\delta_3)$	0.8368	0.9285	0.9736
		λ_3	0.00006	0.00006	0.00006	$\gamma(\lambda_3)$			
4	(0,0,4)	μ_4	-0.00020	-0.00020	-0.00019	$\gamma(\mu_4)$	0.2788	0.2831	0.2843
		λ_4	-0.00007	-0.00005	-0.00004	$\gamma(\lambda_4)$			
5	(3,3,1)*	μ_5	-0.00022	-0.00020	-0.00019	$\gamma(\mu_5)$	1.1211	1.1069	1.0819
		ν_5	-0.00032	-0.00026	-0.00024	$\gamma(\nu_5)$	1.8115	1.9104	1.9240
		δ_5	0.00064	0.00058	0.00055	$\gamma(\delta_5)$	0.9110	0.9660	0.9882
		λ_5	-0.00183	-0.00183	-0.00183	$\gamma(\lambda_5)$	0.0062	0.0312	0.0435
6	(2,2,4)	μ_6	-0.00016	-0.00015	-0.00014	$\gamma(\mu_6)$	0.5894	0.6875	0.7383
		ν_6	0.00026	0.00026	0.00026	$\gamma(\nu_6)$	0.0120	0.0023	-0.0024
		δ_6	-0.00003	-0.00004	-0.00004	$\gamma(\delta_6)$			
		γ_6	-0.00012	-0.00012	-0.00011	$\gamma(\gamma_6)$	0.1326	0.1893	0.2179
		λ_6	0.00004	0.00003	0.00002	$\gamma(\lambda_6)$			
7	(1,1,5)	μ_7	0.00009	0.00009	0.00010	$\gamma(\mu_7)$			
		ν_7	0.00001	0.00001	0.00001	$\gamma(\nu_7)$			
		δ_7	0.00000	-0.00001	-0.00001	$\gamma(\delta_7)$			
		λ_7	-0.00001	-0.00001	-0.00001	$\gamma(\lambda_7)$			
	$\overline{(3,3,3)}$	α_7	0.00006	0.00006	0.00005	$\gamma(\alpha_7)$			
		β_7	0.00000	0.00000	0.00000	$\gamma(\beta_7)$			
8	(4,4,0)*	μ_8	-0.00002	0.00000	0.00000	$\gamma(\mu_8)$			
		ν_8	-0.00013	-0.00011	-0.00011	$\gamma(\nu_8)$	0.9582	0.9260	0.8957
		δ_8	0.00027	0.00025	0.00024	$\gamma(\delta_8)$	0.7319	0.7755	0.7940
		λ_8	0.00107	0.00105	0.00104	$\gamma(\lambda_8)$	0.1332	0.1423	0.1465
13	(5,5,1)*	μ_{13}	-0.00005	-0.00004	-0.00004	$\gamma(\mu_{13})$			
		ν_{13}	0.00001	0.00001	0.00002	$\gamma(\nu_{13})$			
		δ_{13}	0.00013	0.00011	0.00011	$\gamma(\delta_{13})$	0.9835	1.0328	1.0499
		λ_{13}	-0.00059	-0.00058	-0.00057	$\gamma(\lambda_{13})$	0.2270	0.2052	0.1932
18	(6,6,0)*	μ_{18}	-0.00001	0.00000	0.00000	$\gamma(\mu_{18})$			
		ν_{18}	-0.00006	-0.00005	-0.00005	$\gamma(\nu_{18})$			
		δ_{18}	0.00006	0.00005	0.00005	$\gamma(\delta_{18})$			
		λ_{18}	0.00034	0.00033	0.00033	$\gamma(\lambda_{18})$	0.2448	0.1989	0.1748
25	(7,7,1)*	μ_{25}	-0.00002	-0.00001	-0.00001	$\gamma(\mu_{25})$			
		ν_{25}	0.00001	0.00002	0.00002	$\gamma(\nu_{25})$			
		δ_{25}	0.00004	0.00004	0.00004	$\gamma(\delta_{25})$			
		λ_{25}	-0.00021	-0.00020	-0.00020	$\gamma(\lambda_{25})$	0.3781	0.3210	0.2892

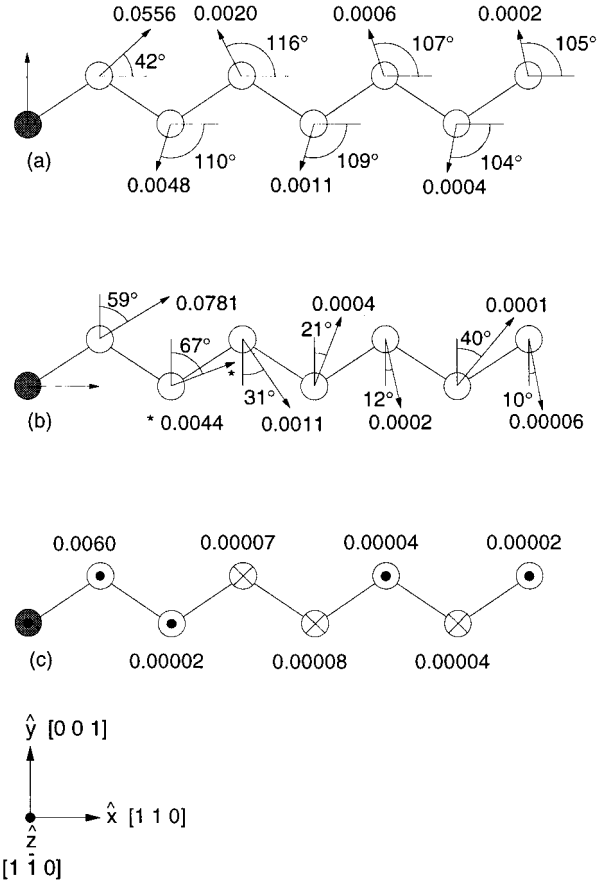

FIG. 1. Forces induced (linear response) along the [1 1 0] zigzag chain by the unit displacement of a generic atom (in grey) of this chain in the (a) [1 1 0], (b) [0 0 1], and (c) [1 1̄ 0] directions. The unit vectors corresponding to these directions are, respectively, $\hat{\mathbf{x}}$, $\hat{\mathbf{y}}$, and $\hat{\mathbf{z}}$. The arrows starting from white atoms represent the direction of the forces, while the absolute value of it is written close to it. Forces along the [1 1̄ 0] direction are indicated by dots, whereas crosses refer to forces in the opposite direction. The forces are expressed in hartree/bohrs.

neighbor shells included. Thus, in the following, we will only reproduce the results obtained without reimposing the acoustic sum rule.

The results are reproduced in Tables II and III. The well-converged calculated frequencies of TA(X) and TA(L) modes are, respectively, 140.46 cm^{-1} and 108.626 cm^{-1} at the calculated equilibrium lattice constant and 147.37 cm^{-1} and 112.86 cm^{-1} at the experimental one. These values are in very good agreement with the experiment in Ref. 25: 149.77 cm^{-1} and 114.41 cm^{-1}.

The associated mode Grüneisen parameters are calculated by

$$\gamma_\sigma = -\frac{d\ln\omega_\sigma}{d\ln V}, \tag{3}$$

where σ is the index of the mode and V is the molar volume (N_A multiplied by the volume of the unit cell) linked to the lattice constant by

TABLE II. Phonon frequencies of TA(X) mode and associated mode Grüneisen parameters for silicon at three different volumes, corresponding to lattice constants a of 10.00, 10.18, and 10.26 bohrs, respectively. The reference value (r.v.) is obtained by taking into account interactions with all the atoms included in the real space box defined by our sampling of the Brillouin zone (ten special points). The other values are obtained by limiting the interactions to the successive nearest-neighbor (NN) shells. The phonon frequencies are expressed in cm^{-1}.

	$\omega_{\mathrm{TA}(X)}$			$\gamma_{\mathrm{TA}(X)}$		
NN	$a=10.00$	$a=10.18$	$a=10.26$	$a=10.00$	$a=10.18$	$a=10.26$
0	383.462	361.688	352.426	1.080	1.102	1.107
1	196.622	206.021	209.256	-1.016	-0.727	-0.598
2	148.056	161.684	166.347	-1.961	-1.340	-1.082
3	135.107	150.376	155.576	-2.413	-1.609	-1.287
4	131.783	147.576	152.949	-2.560	-1.695	-1.352
5	106.607	128.275	135.460	-4.389	-2.633	-2.016
6	105.327	127.507	134.829	-4.557	-2.705	-2.060
7	105.390	127.438	134.725	-4.525	-2.692	-2.053
8	122.392	142.025	148.656	-3.438	-2.180	-1.711
13	128.111	146.863	153.222	-3.131	-2.019	-1.595
18	122.443	142.249	148.906	-3.473	-2.189	-1.710
25	119.535	140.618	147.431	-3.690	-2.280	-1.762
r.v.	119.903	140.466	147.347	-3.690	-2.295	-1.782

$$V = N_A \frac{a^3}{4}. \tag{4}$$

The results, reproduced in Tables II and III, are very sensitive to the volume variations. The calculated mode Grün-

TABLE III. Phonon frequencies of TA(L) mode and associated mode Grüneisen parameters for silicon at three different volumes, corresponding to lattice constants a of 10.00, 10.18, and 10.26 bohrs, respectively. The reference value (r.v.) is obtained by taking into account interactions with all the atoms included in the real space box defined by our sampling of the Brillouin zone (ten special points). The other values are obtained by limiting the interactions to the successive nearest-neighbor (NN) shells. The phonon frequencies are expressed in cm^{-1}.

	$\omega_{\mathrm{TA}(L)}$			$\gamma_{\mathrm{TA}(L)}$		
NN	$a=10.00$	$a=10.18$	$a=10.26$	$a=10.00$	$a=10.18$	$a=10.26$
0	383.462	361.688	352.426	1.080	1.102	1.107
1	147.432	151.460	152.695	-0.609	-0.396	-0.295
2	119.157	127.508	130.363	-1.494	-1.041	-0.845
3	120.881	129.204	132.089	-1.459	-1.033	-0.848
4	124.496	132.393	135.122	-1.346	-0.954	-0.783
5	90.610	103.339	107.667	-3.001	-1.951	-1.547
6	79.247	93.544	98.304	-3.889	-2.390	-1.845
7	76.339	91.167	96.078	-4.197	-2.534	-1.942
8	98.491	110.644	114.798	-2.630	-1.745	-1.396
13	101.679	113.235	117.210	-2.416	-1.628	-1.312
18	96.809	108.985	113.149	-2.680	-1.776	-1.420
25	96.631	108.918	113.746	-2.532	-1.959	-1.737
r.v.	96.239	108.626	112.867	-2.742	-1.814	-1.451

eisen parameters of TA(X) and TA(L) modes are, respectively, -2.295 and -1.814 at the calculated equilibrium lattice constant. These values are not in very good agreement with the experiment in Ref. 26: -1.4 and -1.3. However, if we consider the values -1.782 and -1.451 obtained at the experimental equilibrium lattice constant, the agreement is much better.

Considering for reference the values obtained by taking into account all the atoms included in the real space box we see that the contribution of atoms connected by the zigzag chain along the [1 1 0] direction is the most important for the convergence of the phonon frequencies of TA(X) and TA (L) modes, and of the associated mode Grüneisen parameters. Beyond the fourth atom along the [1 1 0] chain (eighth-nearest neighbors), the contribution of successive nearest neighbors not belonging to the chains is not significant. But the contributions of fifth, sixth, and seventh atoms along the chain (respectively, 13th, 18th, and 25th nearest neighbors) are not negligible in our calculations, contrary to what had been speculated by Wei and Chou.[10] Once more, we emphasize that we have not tested the influence of the pseudopotential and exchange-correlation potential on these contributions.

Including still further atoms along the chains would necessitate using another sampling of the dynamical matrix wave vectors in order to get a bigger real space box. Tables II and III also show that, once interactions with the first-nearest neighbors are included, the anomalous behavior of TA modes at X and L points (negative Grüneisen parameters) is reproduced. This reinforces the pertinence of the model proposed in Ref. 8.

For TA(X) and TA(L) modes, the eigenmodes $u_\sigma(\kappa\alpha)$ are known for any ion from symmetry considerations (see Fig. 2). It is thus even possible to obtain an analytical expression of phonon frequencies from the knowledge of the IFC's.

If we only consider on-site interaction (just atom κ) in the sum of the left-hand side of Eq. (2), we get

$$\omega = \sqrt{\frac{\alpha_0}{m}} \tag{5}$$

for both TA(X) and TA(L) modes, where m is the mass of the silicon ion. The associated mode Grüneisen parameters can easily be obtained by inserting this result in Eq. (3),

$$\gamma = \gamma(\alpha_0), \tag{6}$$

where $\gamma(\alpha_0)$ is the ''force Grüneisen parameter'' that we define as

$$\gamma(\alpha_0) = -\frac{1}{2}\frac{d\ln\alpha_0}{d\ln V}. \tag{7}$$

The force Grüneisen parameters have been listed in Table I for all IFC's whose magnitude is higher than 10^{-4} hartree/bohr^3.

If we consider interactions up to first-nearest-neighbor atom, we get

$$\omega_{\mathrm{TA}(X)} = \sqrt{\frac{\alpha_0 + 4\beta_1}{m}} \tag{8}$$

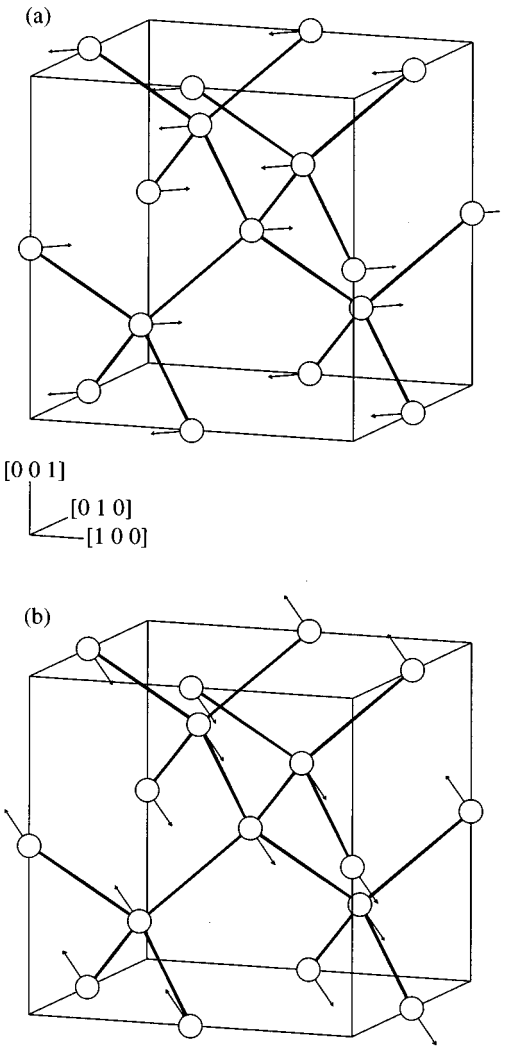

FIG. 2. Vibrational motion corresponding to the (a) TA(X) mode and (b) TA(L) mode in silicon. The displacements of ions are along the [1 1 0] direction in (a) and along the $[11\bar{2}]$ direction in (b).

for the TA(X) mode, and

$$\omega_{\mathrm{TA}(L)} = \sqrt{\frac{\alpha_0 + 2\alpha_1 + 2\beta_1}{m}} \tag{9}$$

for the TA(L) mode. In fact, whatever the number of nearest neighbors taken into account, the phonon frequencies will always be written as the square root of the ratio of a linear combination of the IFC's and the mass. The associated mode Grüneisen parameters can be written as the *weighted sum* of the force Grüneisen parameters corresponding to the IFC's under the radical in Eqs. (8) and (9) . For example, for the TA(X) mode, inserting Eq. (8) in Eq. (3), we get

$$\gamma_{\mathrm{TA}(X)} = -\frac{V}{\sqrt{\alpha_0 + 4\beta_1}}\frac{d\sqrt{\alpha_0 + 4\beta_1}}{dV} = -\frac{1}{2}\frac{V}{\alpha_0 + 4\beta_1}\frac{d\alpha_0 + 4\beta_1}{dV}. \tag{10}$$

This can be rewritten as follows:

$$\gamma_{\mathrm{TA}(X)}=-\frac{1}{2}\left(\frac{\alpha_0}{\alpha_0+4\beta_1}\right)\frac{V}{\alpha_0}\frac{d\alpha_0}{dV}-\frac{1}{2}\left(\frac{4\beta_1}{\alpha_0+4\beta_1}\right)\frac{V}{\beta_1}\frac{d\beta_1}{dV}. \tag{11}$$

The definition of force Grüneisen parameters, Eq. (7), leads to

$$\gamma_{\mathrm{TA}(X)}=\left(\frac{\alpha_0}{\alpha_0+4\beta_1}\right)\gamma(\alpha_0)+\left(\frac{4\beta_1}{\alpha_0+4\beta_1}\right)\gamma(\beta_1) \tag{12}$$

for the TA(X) mode, and

$$\gamma_{\mathrm{TA}(L)}=\left(\frac{\alpha_0}{\alpha_0+2\alpha_1+2\beta_1}\right)\gamma(\alpha_0)+\left(\frac{2\alpha_1}{\alpha_0+2\alpha_1+2\beta_1}\right)\gamma(\alpha_1)+\left(\frac{2\beta_1}{\alpha_0+2\alpha_1+2\beta_1}\right)\gamma(\beta_1) \tag{13}$$

for the TA(L) mode.

Interestingly, the same argument holds whatever the number of nearest neighbors taken into account. And thus, the same kind of formulas will be obtained for phonon frequencies and associated mode Grüneisen parameters.

Indeed, if we consider interactions up to second-nearest neighbor atoms, we get

$$\omega_{\mathrm{TA}(X)}=\sqrt{\frac{\alpha_0+4\beta_1-4\lambda_2}{m}} \tag{14}$$

for the TA(X) mode, and

$$\omega_{\mathrm{TA}(L)}=\sqrt{\frac{\alpha_0+2\alpha_1+2\beta_1-4\nu_2}{m}} \tag{15}$$

for the TA(L) mode. The associated mode Grüneisen parameters can be written as the weighted sum of the force Grüneisen parameters corresponding to the IFC's under the radical in Eqs. (14) and (15):

$$\gamma_{\mathrm{TA}(X)}=\left(\frac{\alpha_0}{\alpha_0+4\beta_1-4\lambda_2}\right)\gamma(\alpha_0)+\left(\frac{4\beta_1}{\alpha_0+4\beta_1-4\lambda_2}\right)\gamma(\beta_1)+\left(\frac{-4\lambda_2}{\alpha_0+4\beta_1-4\lambda_2}\right)\gamma(\lambda_2) \tag{16}$$

for the TA(X) mode, and

$$\gamma_{\mathrm{TA}(L)}=\left(\frac{\alpha_0}{\alpha_0+2\alpha_1+2\beta_1-4\nu_2}\right)\gamma(\alpha_0)+\left(\frac{2\alpha_1}{\alpha_0+2\alpha_1+2\beta_1-4\nu_2}\right)\gamma(\alpha_1)+\left(\frac{2\beta_1}{\alpha_0+2\alpha_1+2\beta_1-4\nu_2}\right)\gamma(\beta_1)+\left(\frac{-4\nu_2}{\alpha_0+2\alpha_1+2\beta_1-4\nu_2}\right)\gamma(\nu_2) \tag{17}$$

for the TA(L) mode.

It should be noted that the weights in Eqs. (12) to (15) are not necessarily included in the interval [0,1] and can thus be negative. This explains why, though almost all force Grüneisen parameters are positive (see Table I), a negative mode Grüneisen parameter can be obtained.

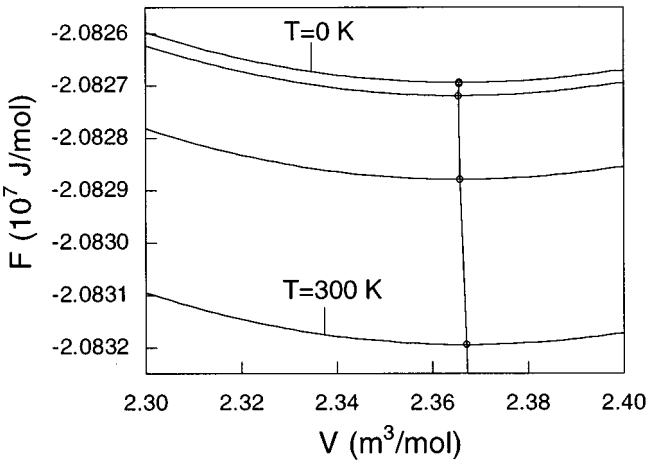

FIG. 3. Volume dependence of the Helmholtz free energy F for four different temperatures. The smallest is 0 K (upper curve); the biggest is 300 K (lower curve), with an increment of 100 K between the curves. The equilibrium volume $V_0(T)$ is located at the minimum of each curve. Between 20 K and 120 K, this volume decreases due to the negative thermal-expansion coefficient.

For example, in Eq. (12), we get for $a=10.18$ bohrs,

$$\gamma_{\mathrm{TA}(X)}=3.08\times 1.1034+(-2.08)\times 1.9817=-0.72, \tag{18}$$

which is just what is obtained in Table II. If all force Grüneisen parameters were equal to 1, we would also get 1 for the mode Grüneisen parameter. This shows that the origin of the negative Grüneisen parameter is the rather important difference between $\gamma(\beta_1)$ and $\gamma(\alpha_0)$.

II. THERMODYNAMIC PROPERTIES

Using the calculated phonon frequencies, the temperature-dependent phonon contribution ΔF to the Helmholtz free energy $F(V,T)$ is calculated as described in Ref. 2. This contribution is added to the energy of the static lattice $E(V)$, calculated previously,[22] to get $F(V,T)$ for a set of three volumes and for various temperatures. This function is then interpolated as a function of V by a second order fit. The equilibrium volumes (or lattice constants) at various temperatures are determined by minimizing $F(V,T)$ as a function of V, as shown in Fig. 3. From $F(V,T)$ any other thermodynamical property can be accessed.

We first analyze briefly the specific effect of the zero-point motion. We find that the zero-point contribution to Helmholtz free energy F is $\Delta F_0=12$ J/mol, which is about 2.5% of the cohesive energy [460 kJ/mol (Ref. 27)]. This zero-point contribution causes the lattice constant to be shifted from 10.1894 bohrs to 10.1974 bohrs, which is a change smaller than 0.1%, and the bulk modulus B_T from 1.0387 Mbar to 1.0292 Mbar, which is a change of 1%. Note, however, that the change in the bulk modulus includes two effects: first, it is linked to the second derivative of $F(V)$ that includes the zero-point motion contribution ΔF_0; and second, it is calculated for a different volume due to the shift of the lattice constant. In Fig. 4, we present the temperature

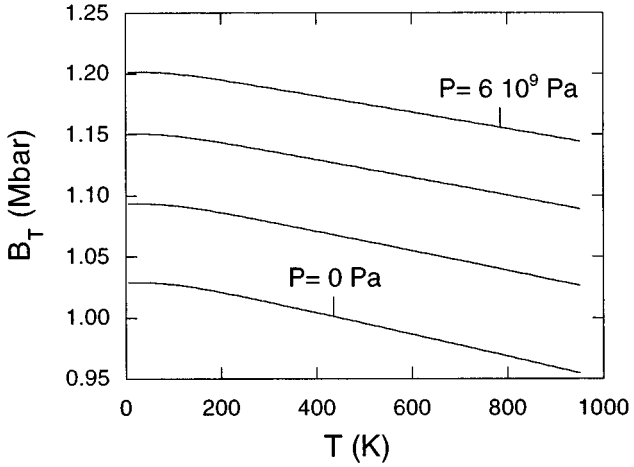

FIG. 4. Temperature dependence of the theoretical bulk modulus B_T for four different pressures. The smallest is 0 Pa (lower curve); the biggest is 6×10^9 Pa (upper curve), with an increment of 2×10^9 Pa between the curves. B_T is expressed in Mbar. Temperature is in K.

dependence of B_T for different pressures.

The entropy can be calculated following Ref. 2. We get $S(298.15\ \mathrm{K})=19.3\ \mathrm{J\ K^{-1}\ mol^{-1}}$, to be compared to the experimental value of 18.81 J K^{-1} mol^{-1}.[28] We have also calculated the variation of enthalpy $H=F+TS-PV$ between 0 and 298.15 K. We get 3.285 J mol^{-1}, whereas the experimental value is 3.217 J mol^{-1}.[28] We present in Fig. 5 the molar constant-pressure specific heat $C_{P,m}$ for various pressures. This result agrees quite well with experimental work.[29,30] It is interesting to note that, for temperatures higher than 85 K, $C_{P,m}$ is higher for low values of the pressure, whereas for temperatures lower than 85 K, it is just the contrary. This means that there exists a temperature around 85 K for which $C_{P,m}$ is independent of pressure. In order to understand this observation, we use the following relation (see Ref. 31):

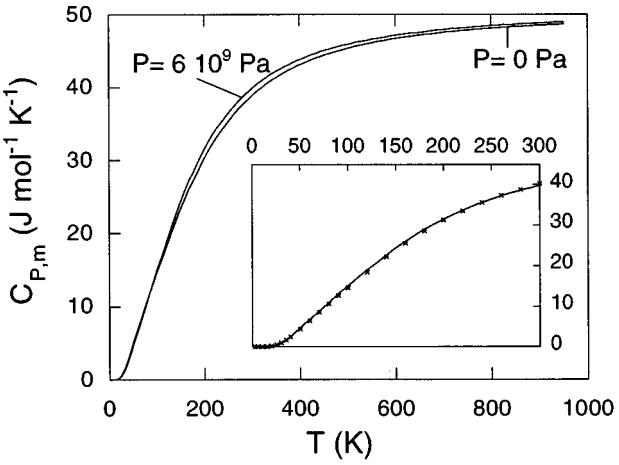

FIG. 5. Temperature dependence of the constant-pressure specific heat $C_{P,m}$ for two different pressures. The smallest is 0 Pa (upper curve at high temperature), the biggest is 6×10^9 Pa (lower curve at high temperature). $C_{P,m}$ is expressed in J mol^{-1} K^{-1}. The crosses indicate experimental data (Ref. 29). Temperature is in K.

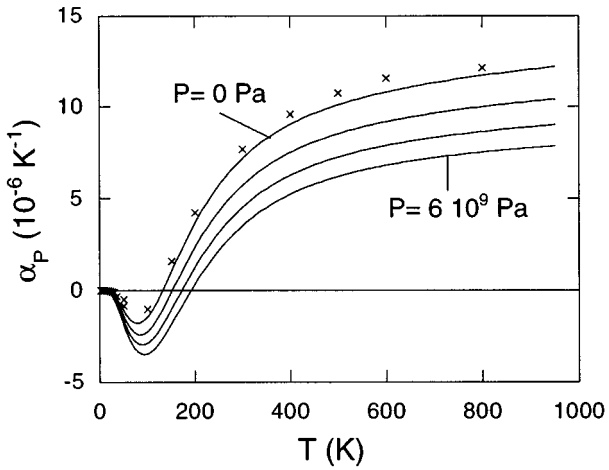

FIG. 6. Temperature dependence of the volumic thermal-expansion coefficient α_P for four different pressures. The smallest is 0 Pa (upper curve); the biggest is 6×10^9 Pa (lower curve), with an increment of 2×10^9 Pa between the curves. α_P is expressed in K^{-1}. The crosses indicate experimental data (Ref. 28). Temperature is in K.

$$\left(\frac{\partial S}{\partial P}\right)_T=-\left(\frac{\partial V}{\partial T}\right)_P \tag{19}$$

to write

$$\left(\frac{\partial C_{P,m}}{\partial P}\right)_T=T\left(\frac{\partial^2 S}{\partial P\,\partial T}\right)=-T\left(\frac{\partial^2 V}{\partial T^2}\right)_P$$
$$=-TV\left[\alpha_P^2+\left(\frac{\partial \alpha_P}{\partial T}\right)_P\right]. \tag{20}$$

This shows that in order to have $C_{P,m}$ independent of pressure, one must have a decreasing α_P. This is precisely the case of silicon between 20 K and 100 K, where the thermal-expansion coefficient gets more and more negative.

This thermal-expansion coefficient is well reproduced by our calculations (see Fig. 6). It is worth noting that increasing the pressure reinforces the anomalous negative behavior of this property. This is confirmed by the strong negative value of the overall Grüneisen parameter at high pressure (see Fig. 7). This anomalous behavior also has consequences for other properties. We present in Fig. 8 the difference $C_{P,m}-C_{V,m}$ between the molar constant-pressure specific heat $C_{P,m}$ and the molar constant-volume specific heat $C_{V,m}$ for various pressures. At high temperature $C_{P,m}-C_{V,m}$ increases with increasing pressure, while at low temperature, it is the contrary and the curve presents a bump. This can be deduced from the following relation:[31]

$$C_{P,m}-C_{V,m}=\frac{\alpha_P^2 VT}{\kappa_T}, \tag{21}$$

where $\kappa_T=1/B_T$. Similarly, the difference B_S-B_T between B_S the bulk modulus calculated from F at constant entropy and B_T the bulk modulus calculated from F at constant temperature presents the same behavior as $C_{P,m}-C_{V,m}$ as shown in Fig. 9. Indeed, we can write[31]

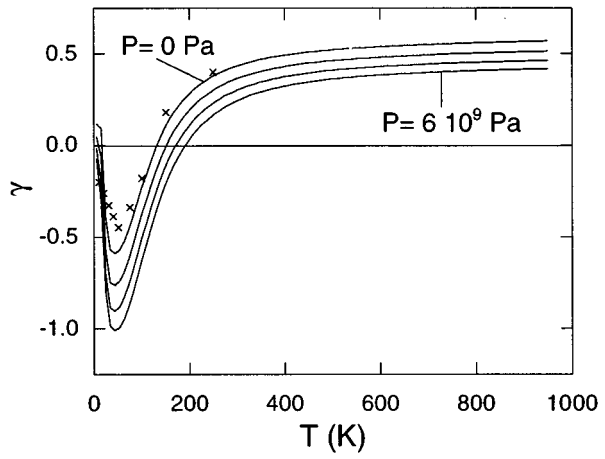

FIG. 7. Temperature dependence of overall Grüneisen parameter γ for four different pressures. The smallest is 0 Pa (upper curve), the biggest is 6×10^9 Pa (lower curve), with an increment of 2×10^9 Pa between the curves. The crosses indicate experimental data (Ref. 33). Temperature is in K.

$$\kappa_S-\kappa_T=\frac{\alpha_P^2VT}{C_{P,m}}, \tag{22}$$

where $\kappa_S=1/B_S$.

III. ATOMIC TEMPERATURE FACTOR

At finite temperature T, the intensity of x-ray diffraction from the crystal is reduced, due to atomic motion. The atomic temperature factor $e^{-W(\kappa)}$ characterizes the oscillations of atom κ around its equilibrium position. It is defined[32] by

$$e^{-W(\kappa)}=\exp\left(-\frac{1}{2}\sum_{\alpha\beta}B_{\alpha\beta}(\kappa)G_\alpha G_\beta\right), \tag{23}$$

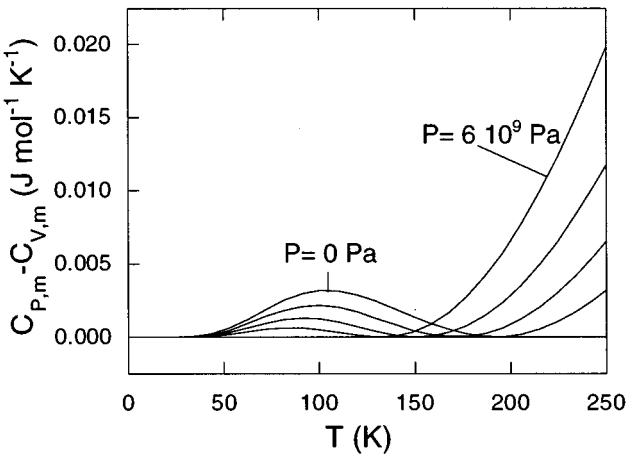

FIG. 8. Temperature dependence of the difference between the constant-pressure specific heat $C_{P,m}$ and the constant-volume specific heat $C_{V,m}$ for four different pressures. The smallest is 0 Pa (lower curve at high temperature), the biggest is 6×10^9 Pa (upper curve at high temperature), with an increment of 2×10^9 Pa between the curves. $C_{P,m}$ is expressed in J mol^{-1} K^{-1}.

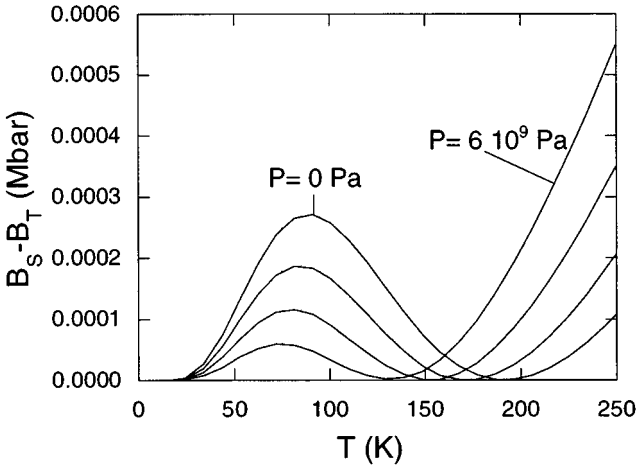

FIG. 9. Temperature dependence of the difference between B_S the bulk modulus calculated from F at constant entropy and B_T the bulk modulus calculated from F at constant temperature, for four different pressures. The smallest is 0 Pa (lower curve at high temperature); the biggest is 6×10^9 Pa (upper curve at high temperature), with an increment of 2×10^9 Pa between the curves. B_S-B_T is expressed in Mbar. Temperature is in K.

where G_α is the component of scattering wave vector **G** which is a reciprocal lattice vector, and $B_{\alpha\beta}(\kappa)$ is the mean-square atomic displacement[2] of atom κ along the directions α and β:

$$B_{\alpha\beta}(\kappa)=\frac{1}{N_AM_\kappa}\sum_{\mathbf{q},l}\frac{\hbar}{2\omega(\mathbf{q},l)}\coth\frac{\hbar\omega(\mathbf{q},l)}{2k_BT}\times e_i(\kappa|\mathbf{q},l)e_j^*(\kappa|\mathbf{q},l), \tag{24}$$

where M_κ is the mass of atom κ, and $e_i(\kappa|\mathbf{q},l)$ is the ith component of the eigenvector associated with mode l at **q** in the lattice coordinates.

In the case of silicon, there is only one kind of atom. Thus, for all atoms $e^{-W(\kappa)}$ is identical. The reduction of the diffusion intensity is given by $e^{-2W(\kappa)}$, which is usually called the Debye-Waller factor. The symmetry of the diamond structure imposes that

$$B_{\alpha\beta}(\kappa)=B\delta_{\alpha\beta}. \tag{25}$$

(This B is not to be confused with the bulk modulus.)

In Table IV, the results obtained for the mean-square atomic displacement, at three different volumes, corresponding to lattice constants a of 10.00, 10.18, and 10.26 bohrs, respectively, are compared with experimental results. The agreement is on the order of a few percent.

Interestingly, even at room temperature, the mean-square atomic displacement decreases with increasing volume, contrary to intuition. This can easily be understood from the definition of B [see Eq. (24)]. Indeed, it is written as a sum over all phonon bands of a term which is proportional to the inverse square of the frequency of the mode ω^{-2} (since $\coth x\rightarrow x^{-1}$ for small x). Thus, it is determined mostly by acoustic branches. This is confirmed by a band-by-band decomposition of B (see Table IV), where the two lowest bands account for more than 2/3 of B. As the TA band and the first longitudinal-acoustic (LA) band exhibit a negative mode

TABLE IV. Mean-square atomic displacement B of silicon atoms at $T=295$ K for three different volumes (lattice constants a of 10.00, 10.18, and 10.26 bohrs), and the corresponding experimental data at $a=10.26$ bohrs. The lower part of the table presents a band-by-band decomposition of B. The values are expressed in Å^2.

	Present work			Experimental data ($a=10.26$)			
	$a=10.00$	$a=10.18$	$a=10.26$	Ref. 34	Ref. 35	Ref. 36	Ref. 37
B	0.4967	0.4745	0.4707	0.4613	0.4500	0.4515	0.4660
B(TA)	0.2298	0.2052	0.1992				
$B(\text{LA}_1)$	0.1592	0.1510	0.1482				
$B(\text{LA}_2)$	0.0496	0.0543	0.0563				
B(LO+TO)	0.0582	0.0641	0.0672				

Grüneisen parameter, we see that their contribution to B decreases with increasing volume, contrary to the contribution of the second LA band and optic bands.

The thermal parameter B and the atomic temperature factor $e^{-W(\kappa)}$, for diffraction with scattering vector $\mathbf{G}=(2\pi/a_0)\hat{\mathbf{z}}$, are also calculated as a function of temperature (see Figs. 10 and 11). The atomic temperature factor is not 1 even at 0 K due to the zero-point motion.

CONCLUSIONS

In this paper, dynamical properties of silicon have been calculated using a variational approach to density-functional perturbation theory. We have presented an *ab initio* study of the volume dependence of interatomic force constants up to 25th nearest neighbors. Phonon frequencies of TA(X) and TA(L) modes, and of the associated mode Grüneisen parameters, have also been calculated for different volumes. The influence of successive nearest-neighbor shells has been analyzed. This study has confirmed that the contribution of atoms connected by the zigzag chain along the [1 1 0] direction is the most important. It has also proven that the contributions of fifth, sixth, and seventh atoms along the chain (respectively, 13th, 18th, and 25th nearest neighbors) are not negligible. Analytical formulas, taking into account interactions up to second-nearest neighbors, have been developed for phonon frequencies of TA(X) and TA(L) modes and the corresponding mode Grüneisen parameters. The volume and pressure dependence of various thermodynamic properties (specific heat, bulk modulus, and thermal expansion) were also analyzed. We have pointed out the effect of the negative mode Grüneisen parameters of the acoustic branches on these properties. The effect of zero-point motion was also investigated. Finally, we have presented the evolution of the mean-square atomic displacement and of the atomic temperature factor with the temperature for different volumes, emphasizing the anomalous effects due to the negative mode Grüneisen parameters, present at all investigated temperatures.

ACKNOWLEDGMENTS

We thank J.-M. Beuken for permanent computer assistance. The ground state results were obtained using a version of the software program PLANE-WAVE (written by D.C. Allan), which is marketed by Biosym Technologies of San Di-

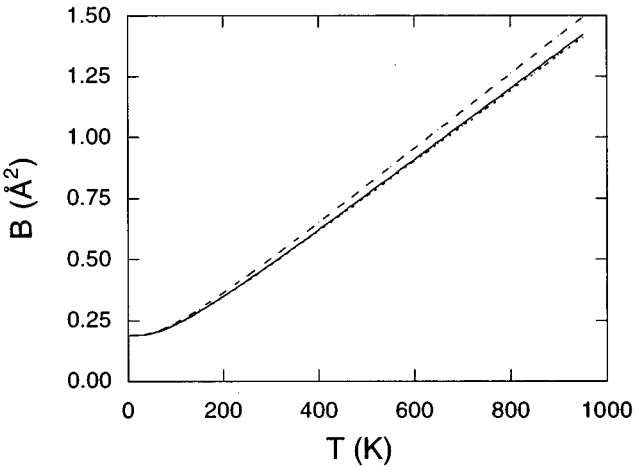

FIG. 10. Temperature dependence of mean-square atomic displacement B for silicon atoms in bulk silicon at three different volumes, corresponding to lattice constants a of 10.00 (dashed line), 10.18 (solid line), and 10.26 bohrs (dotted line), respectively. The values of B are expressed in Å^2. Temperature is in K.

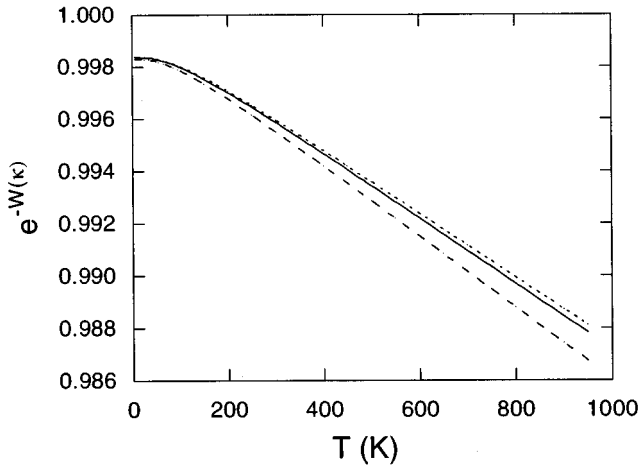

FIG. 11. Temperature dependence of atomic temperature factor $e^{-W(\kappa)}$ for silicon atoms in bulk silicon for diffraction with the scattering vector $\mathbf{G}=(2\pi/a_0)\hat{\mathbf{z}}$ at three different volumes, corresponding to lattice constants a of 10.00 (dashed line), 10.18 (solid line), and 10.26 bohrs (dotted line), respectively. Temperature is in K.

ego. Two of the authors (G.-M. R., and X.G.) have benefited from financial support of the National Fund for Scientific Research (Belgium). This paper presents research results of the Belgian Program on Interuniversity Attraction Poles initiated by the Belgian State, Prime Minister's Office, Science Policy Programming. We also acknowledge the use of the RS 6000 workstation from the common project between IBM Belgium, UCL, and FUNDP.

[1] See P. Giannozzi, S. de Gironcoli, P. Pavone, and S. Baroni, Phys. Rev. B **43**, 7231 (1991); K. Karch *et al.*, *ibid.* **50**, 17 054 (1994), and references therein.
[2] C. Lee and X. Gonze, Phys. Rev. B **51**, 8610 (1995).
[3] L. L. Boyer, Phys. Rev. Lett. **42**, 584 (1979).
[4] M.-M. Kagaya, N. Shuoji, and T. Soma, Solid State Commun. **65**, 1445 (1988).
[5] S. Biernacki and M. Scheffler, Phys. Rev. Lett. **63**, 290 (1989).
[6] A. Fleszar and X. Gonze, Phys. Rev. Lett. **64**, 2961 (1990).
[7] S. Baroni, P. Gianozzi, and A. Testa, Phys. Rev. Lett. **58**, 1861 (1987).
[8] C. H. Xu, C. Z. Wang, C. T. Chan, and K. M. Ho, Phys. Rev. B **43**, 5024 (1991).
[9] S. Wei, C. Li, and M. Y. Chou, Phys. Rev. B **50**, 14 587 (1994).
[10] S. Wei and M. Y. Chou, Phys. Rev. B **50**, 2221 (1994).
[11] S. Wei and M. Y. Chou, Phys. Rev. Lett. **69**, 2799 (1992).
[12] A. Mazur and J. Pollmann, Phys. Rev. B **39**, 5261 (1989).
[13] D. J. Chadi and M. L. Cohen, Phys. Rev. B **8**, 5747 (1973).
[14] X. Gonze, D. C. Allan, and M. P. Teter, Phys. Rev. Lett. **68**, 3603 (1992).
[15] X. Gonze, J.-C. Charlier, D. C. Allan, and M. P. Teter, Phys. Rev. B **50**, 13 035 (1994).
[16] W. Kohn and L. J. Sham, Phys. Rev. **140**, A1133 (1965).
[17] M. P. Teter, M. C. Payne, and D. C. Allan, Phys. Rev. B **40**, 12 255 (1989).
[18] M. C. Payne *et al.*, Rev. Mod. Phys. **64**, 1045 (1992).
[19] M. P. Teter (unpublished).
[20] D. M. Ceperley and B. J. Alder, Phys. Rev. Lett. **45**, 566 (1980).
[21] D. R. Hamann, Phys. Rev. B **40**, 2980 (1989).
[22] G.-M. Rignanese *et al.*, Phys. Rev. B **52**, 8160 (1995).
[23] F. Herman, J. Phys. Chem. Solids **8**, 405 (1959).
[24] See Eq. (3.10) in R. M. Pick, M. H. Cohen, and R. M. Martin, Phys. Rev. B **1**, 910 (1970).
[25] G. Dolling, in *Inelastic Scattering of Neutrons in Solid and Liquids*, edited by S. Ekland (IAEA, Vienna, 1963), Vol. II.
[26] B. A. Weinstein and G. J. Piermarini, Phys. Rev. B **12**, 1172 (1975).
[27] S. G. Davis, D. F. Anthrop, and A. W. Searcy, J. Phys. C **19**, 3163 (1986).
[28] *Physics of Group IV and III-V Compounds*, Vol. 17 of *Landolt-Börnstein: Numerical Data and Functional Relationships in Science and Technology*, edited by O. Madelung (Springer-Verlag, Berlin, 1982).
[29] P. Flubacher, A. J. Leadbetter, and J. A. Morrison, Philos. Mag. **4**, 273 (1959).
[30] P. D. Desai, J. Phys. Chem. Ref. Data **15**, 967 (1986).
[31] H. B. Callen, *Thermodynamics and an Introduction to Thermostatistics* (John Wiley & Sons, Inc., New York, 1985).
[32] B. T. M. Willis and A. W. Pryor, *Thermal Vibrations in Crystallography* (Cambridge University Press, Cambridge, 1975).
[33] H. Ibach, Phys. Status Solidi **31**, 625 (1969).
[34] P. J. E. Aldred and M. Hart, Proc. R. Soc. London Ser. A **332**, 239 (1973).
[35] H. A. Graf, J. R. Schneider, A. K. Freund, and M. S. Lehmann, Acta Crystallogr. Sec. A **37**, 863 (1981).
[36] M. Fehlmann, J. Phys. Soc. Jpn. **47**, 225 (1979).
[37] K. Krec and V. Steiner, Acta Crystallogr. Sec. A **40**, 459 (1984).